JOURNAL OF MATERIALS SCIENCE **34** (1999) 5469–5476

XTEM study of Al doped TiO_2 anatase epitaxial films deposited on MgO by pulsed laser deposition

V. S. TEODORESCU
National Institute for Physics of Materials, P.O. Box Mg-7 Bucharest-Magurele, 76900 Bucharest, Romania

M. G. BLANCHIN*
Département de Physique des Matériaux, CNRS UMR 5586, Université Claude-Bernard, 69622 Villeurbanne Cedex, France

C. GARAPON
Laboratoire de Physicochimie des Matériaux Luminescents, CNRS UMR 5620, Université Claude-Bernard, 69622 Villeurbanne Cedex, France

C. CHAMPEAUX
Laboratoire de Matériaux Céramiques et Traitements des Surfaces, CNRS ESA 6015, Université de Limoges, 87060 Limoges Cedex, France

Al doped TiO_2 anatase films epitaxially grown by Pulsed Laser Deposition (PLD) on MgO single crystal substrates have been studied by cross-section transmission electron microscopy. The main structural features of such films are the columnar morphology of the anatase grains and the formation of a spinel buffer layer at the TiO_2/MgO interface. The spinel layer is Al rich and displays a steep gradient in Mg composition. Correlation between the microstructure and the optical properties of the films is presented also.

1. Introduction

Titanium dioxide films, generally used for antireflection coatings or corrosion-resistant coatings, have become very interesting for integrated optics applications. Different techniques based on electron beam evaporation [1], sol-gel method [2, 3], plasma enhanced chemical vapour deposition [4] and finally Pulsed Laser Deposition (PLD) methods [5–8] were used for fabrication of TiO_2 thin films. The microstructure of such films is sensitive to their composition which also induces changes in the optical properties. Transmission electron microscopy (TEM) is for the moment the most complete method to investigate the morphology and the structure of thin films, especially using the cross section technique (XTEM). This paper reports the structural features observed by XTEM in the case of Al doped TiO_2 anatase thin films deposited by PLD on MgO single crystals. Systematic study of TiO_2 films deposited by PLD on different substrates in view of waveguiding applications is reported separately [9].

2. Experimental

Thin film deposition was done by laser ablation of a rotating target prepared from TiO_2 rutile powder mixed with about 11% Al_2O_3 powder (concentration expressed in ratio of oxide molecules), pressed and sintered at 1050 °C. A KrF excimer laser with a fluency of 3 J/cm^2 was used. In the present case the films were deposited on the carefully cleaned (001) cubic face of MgO single crystals; the temperature of the substrate was maintained at 790 °C during deposition achieved under a 0.1 mbar oxygen pressure. Details on the experimental set-up and the deposition procedure have been already published [8, 10].

Thin foils for TEM were prepared from the specimens by a standard cross-section technique [11, 12]. The cutting direction used for the specimen preparation was selected along the [001] direction of the MgO cubic substrate. This allowed the TiO_2/MgO interface to be observed along the [100] direction. Specimens were mechanically polished down to a thickness of about 30 μm using the tripod method. The final ion milling was performed by means of a Gatan equipment working with two argon ion guns operated at 4 keV.

The TEM studies were achieved in a Topcon 002B transmission electron microscope operated at 200 kV. Both conventional imaging and electron diffraction modes were used to investigate the structure of cross-sections of the whole film on the substrate. The crystal

* Author to whom all correspondence should be addressed.

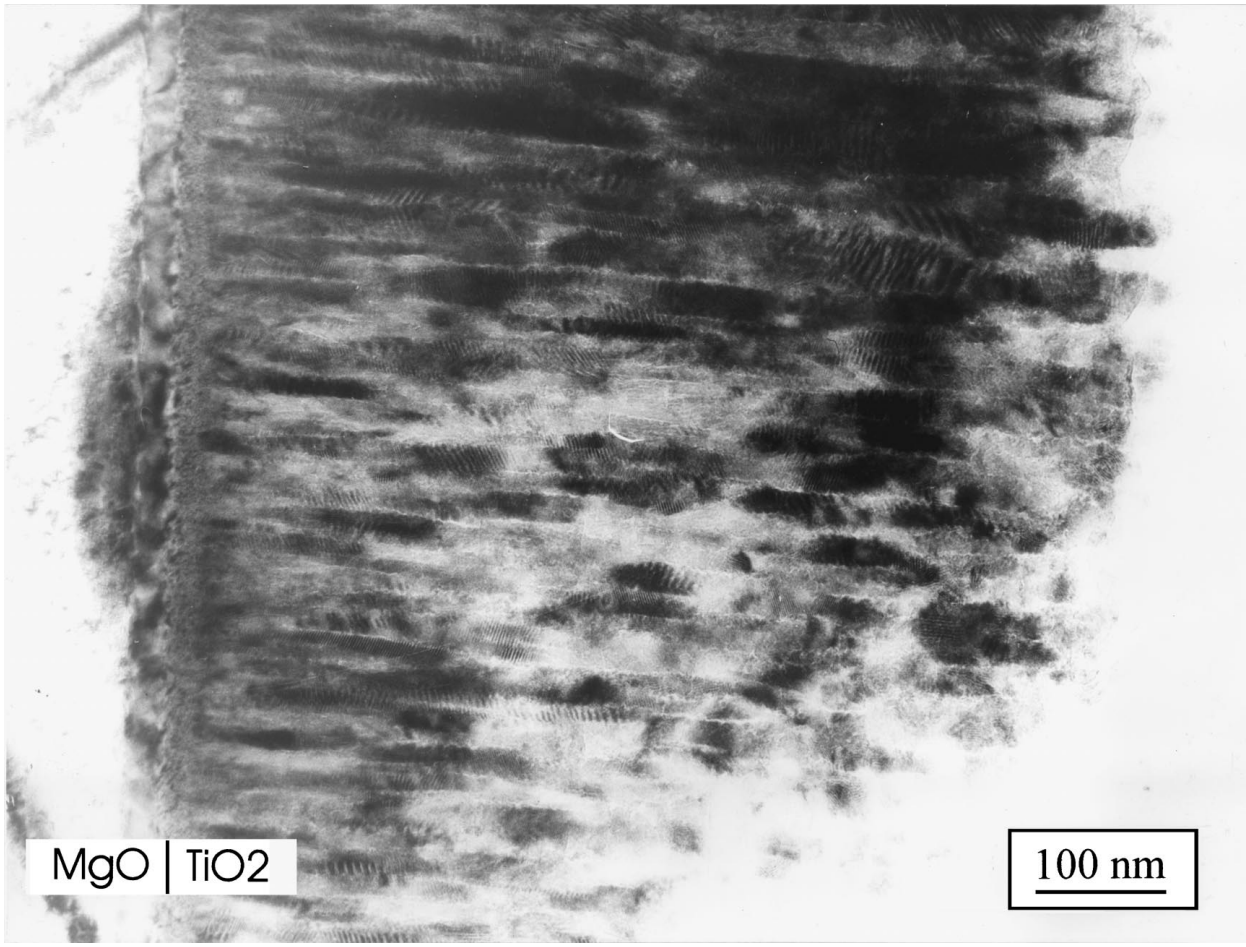

Figure 1 Medium magnification TEM image showing the whole cross-section of the TiO_2 anatase film on the (001) MgO substrate; the film/substrate interface is delineated.

lattices of the film and of the substrate were also imaged at 0.18 nm spatial resolution using the so called high resolution (HR) imaging mode i.e. the atomic columns parallel to the observation axis being seen at high magnification as white or dark spots [12]. Correlatively the concentration of the chemical elements was analysed in situ in the microscope by means of Energy Dispersive X-Ray spectrometry (EDX) [12].

3. Results

3.1. Structural features of the films

The general aspect of the TiO_2 films can be seen on medium magnification cross-section images showing the whole film deposited on the substrate together with the film/substrate interface (Fig. 1). Clearly the film is polycrystalline with a columnar morphology. The thickness of the film across ~ 1 μm (the scale of low magnification observations) looks uniform, in the present case about 800 nm.

Selected area electron diffraction (SAED) patterns (Fig. 2a) corresponding to such images reveal the mosaic formed by the columnar grains. The intense systematic reflections arising from all the parts of the columnar region belong to anatase, the low temperature phase of TiO_2: the structure is tetragonal, space group I41/amd (group number 141), with cell parameters: $a = b = 0.37852$ nm and $c = 0.95139$ nm. (JCPDS 21-1272). Weak supplementary reflections corresponding to interplanar distances of 0.378 and 0.325 nm (Fig. 2a) are found to arise scarcely. The first one corresponds to 001 reflection of anatase which is theoretically forbidden but does appear here for reasons discussed later. The second one belongs to rutile, another TiO_2 phase found as traces in the film. In the bottom part of the columnar region, some reduced cubic phases which can be $TiO_{1.25}$ ($a = 0.417$ nm) or the Al substituted parent phases $(Ti,Al)O_{1+x}$ are detected by diffraction (see SAED pattern in Fig. 2b). Careful examination of many SAED patterns obtained from the columnar mosaic did not provide any consistent data for the existence of any pure aluminium oxide.

From SAED patterns like in Fig. 2 it can be determined that the average orientation of the columnar mosaic is epitaxial, the columnar axis being perpendicular to the interface plane and nearly parallel to the [001] axis of anatase. The crystallographic relationships between anatase and MgO are closed to cube to cube, i.e. $[001]TiO_2$ // [001]MgO and $[100]TiO_2$ // [100]MgO (Fig. 2).

Conventional TEM images at higher magnification (Fig. 3) exhibit rather uniformly distributed moiré fringes [13]. These moiré fringe patterns are mainly rotational [13], generated by interference between 011 reflections, due to the superposition of adjacent grains viewed in projection. Analysis of the distribution of the moiré fringe spacings D (Fig. 4) gives quantitative information [13] about the corresponding angular

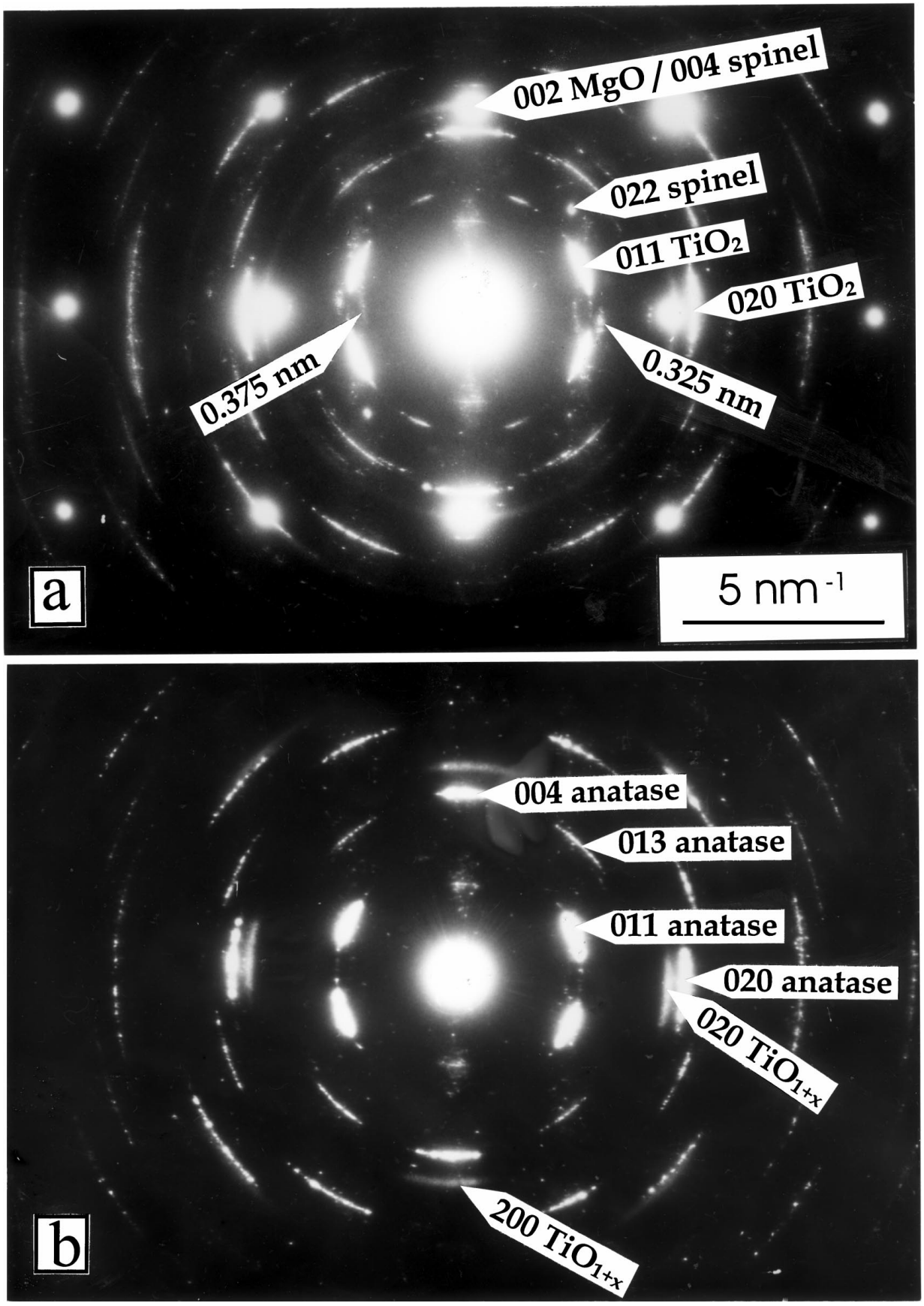

Figure 2 SAED pattern from the whole cross-section TiO_2 film/MgO substrate (a), and SAED pattern selected from the bottom part of the columnar region of the film (b). These patterns correspond to the [100] zone axis of the structures.

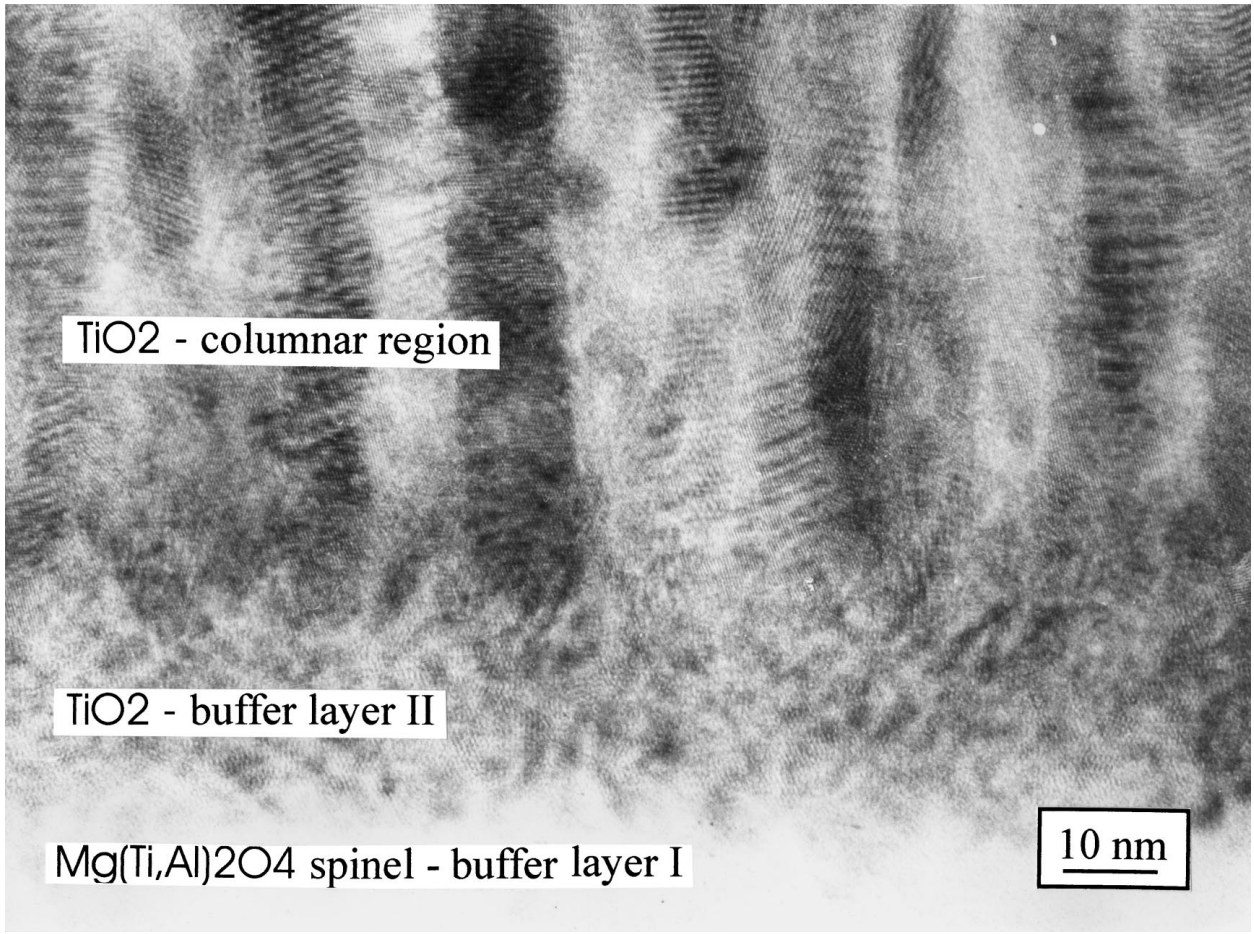

Figure 3 Higher magnification TEM image from the bottom part of the columnar mosaic structure, exhibiting the moiré fringe contrasts.

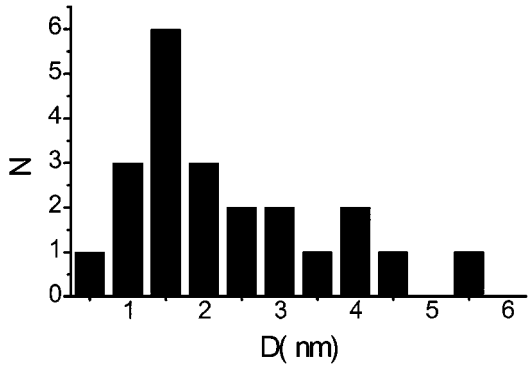

Figure 4 Histogram of the moiré fringe spacings.

dispersion of the adjacent anatase grains with respect to the [001] axis orientation. This dispersion is frequently less than 10° ($D > 2$ nm), as confirmed by SAED; however the [001] lattice direction in some grains is inclined by more than 20° ($D < 1$ nm) with respect to the film/substrate interface normal.

The diameter of the columnar grains exhibits a narrow distribution which is depicted in Fig. 5. At the bottom part of the film (distance less than 100 nm from the substrate), the columnar grains have an average diameter of 12.5 nm. The average diameter increases up to 15 nm at the top part of the film. About 70% of the columnar grains have their length practically equal to the thickness of the film. During their growth the columnar grains nevertheless accommodate some lattice

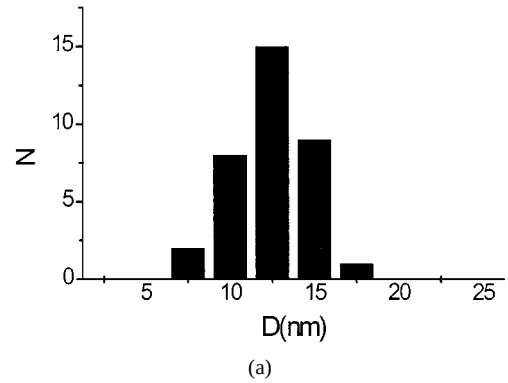

(a)

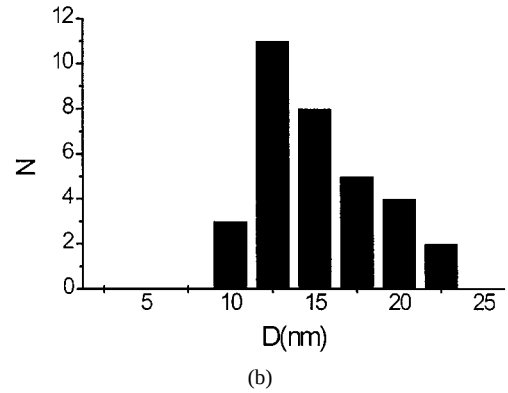

(b)

Figure 5 Histogram of the columnar grain diameters: (a) bottom part of the TiO_2 film (at 100 nm distance from the interface); (b) top part of the film (at 600 nm distance from the interface).

defects and this limits the size of the coherent lattice domains to about 300–400 nm, as revealed by the Bragg contrast in the conventional images (Figs 1 and 3).

3.2. Film/substrate interface

Figs 1 and 3 show the existence of a complicate buffer layer at the interface between the film and the substrate. The nature of that buffer layer has been investigated further by subsequent ion thinning of the specimens, in order to keep only the buffer layer at the limit of the thinned foil.

High magnification HRTEM images like in Fig. 6, give detailed views of the buffer layer which consists in two parts (see also Fig. 3). The first part (labelled I) close to the MgO substrate is a single crystal layer (about 30 nm wide) of spinel: in the corresponding SAED pattern (Fig. 7a), the spinel structure is evidenced by the presence of the 220_{spinel} reflections appearing in the place of the 110_{MgO} forbidden reflections: so the orientation relationship of the spinel with respect to the MgO substrate is cube to cube. Weak supplementary reflections significant of ordered lattice defects and/or ordered aluminium atoms, are seen also on the same pattern (Fig. 7a): this will be discussed in the next section. The second part (II) of the buffer layer (Figs 3 and 6), about 20 nm wide, consists of nanometric size crystallites of anatase oriented in all the possible cube to cube orientations with respect to MgO and spinel (see SAED pattern in Fig. 7b).

Associated with XTEM imaging, EDX spectrometry was performed using an electron beam diameter of 10 nm, to analyse the composition of the film: the corresponding ratios of metal atomic concentrations are displayed in Table I. These measurements indicate an excess of Al in the spinel region. The value of the atomic ratio Al/Ti is 0.25 in the columnar region, 0.27 at the top of the buffer layer and increases up to 0.58 in the spinel region. Actually the average value of the Al/Ti ratio over the film cross-section is consistent with the molecular oxide ratio Al_2O_3/TiO_2 (about 0.11) in the alumina/rutile target. On the other hand the Mg concentration varies significantly across the spinel buffer layer: the Mg/Ti ratios displayed in Table I are consistent with two different spinel compounds which are $(Ti,Al)_2MgO_4$ at the top part and $(Ti,Al)Mg_2O_4$ at the bottom part of the spinel layer.

TABLE I Ratios of the metal atomic concentrations in different regions of the TiO_2/MgO cross-section (the Ti atomic concentration being normalized to the unity)

Region	Atomic ratio Mg/Ti	Atomic ratio Al/Ti
Columnar region of the anatase film	0	0.25
Buffer layer II	0. 1	0.27
Buffer layer I/spinel top part	0.37	0.58
Buffer layer I/spinel bottom part	2.12	0.58

Finally a schematic drawing of the columnar film together with the buffer layer sandwich, is reproduced in Fig. 8, where the orientations of the various structures are depicted by icons.

3.3. Film surface

The surface of the films is not smooth; the top part of the cross-section looks like a palisade. This is due to the fact that the surface terminations of the columnar grains are the natural anatase habit planes (101) and (103), as seen on the HRTEM image in Fig. 9. On the HRTEM images from the columnar region (like in Figs 3 and 9) it is also observed that the {101} lattice planes are continuous through several adjacent columnar grains. This suggests that the grains are arranged in bundles of closely oriented columns: such bundles can be 3 to 5 grains wide, i.e. about 50 to 100 nm, in agreement with results of AFM experiments [9].

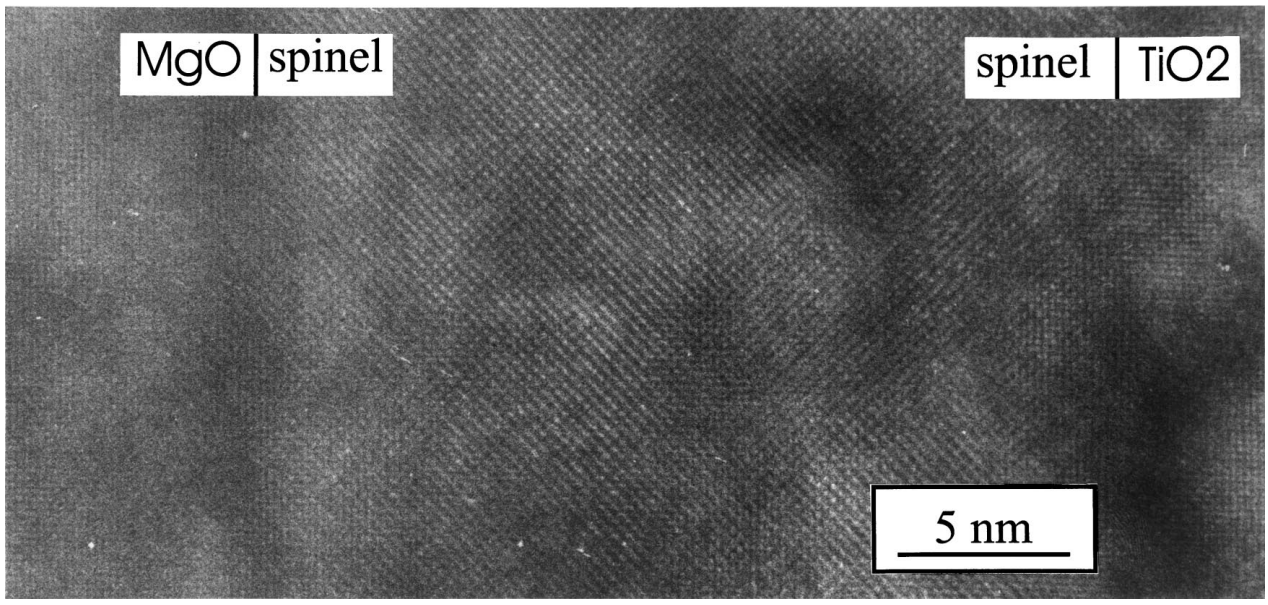

Figure 6 HRTEM image of the buffer layer at the film/substrate interface.

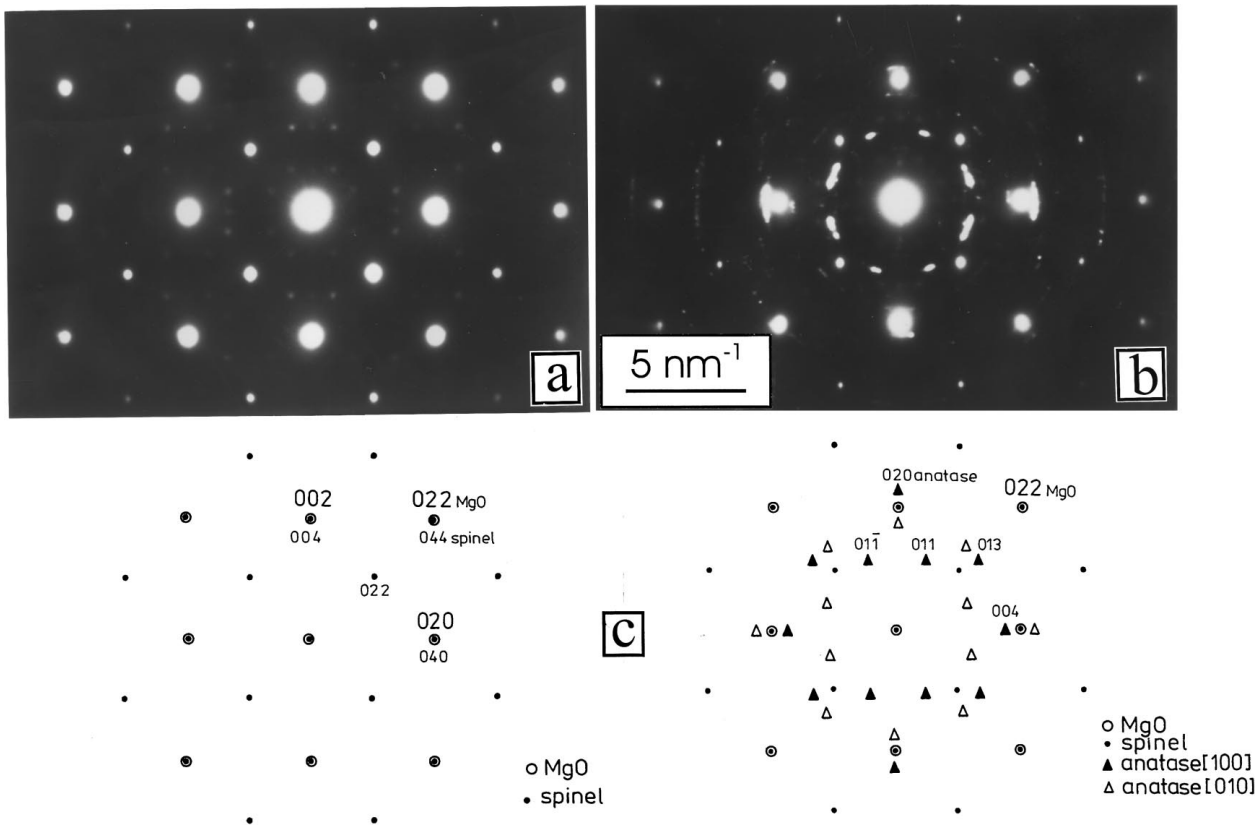

Figure 7 SAED patterns corresponding to the buffer layer region in Fig. 6: (a) bottom part of the buffer layer (MgO + spinel structures); (b) top part of the buffer layer (spinel + TiO_2 structures); (c) indexation of the reflections in the experimental patterns (a) and (b).

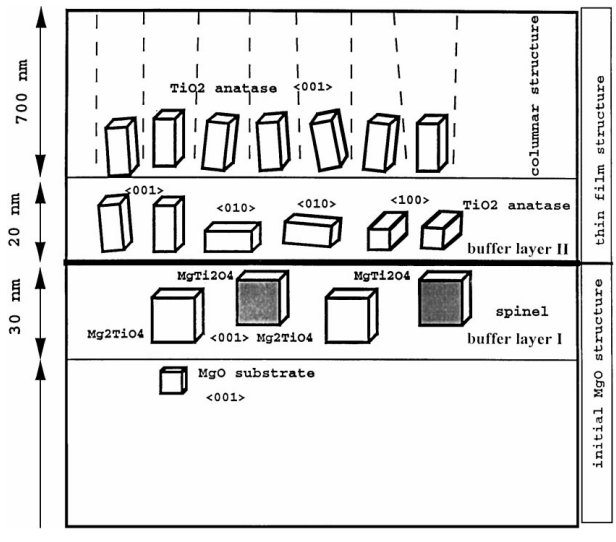

Figure 8 Schematic drawing for the orientation of the different structures in the columnar mosaic and in the buffer layer. The corresponding unit cells are represented as icons. Labelling like "⟨**100**⟩ anatase" indicates that the ⟨001⟩ direction of anatase in that crystal is parallel to the ⟨**100**⟩ direction of the MgO substrate (the interface plane being parallel to the (001) plane of MgO).

3.4. Optical properties

A systematic study of TiO_2 films obtained by PLD deposition on various substrates was achieved in view of waveguiding applications [9]. Optical properties of the films were then investigated, i.e. refractive index and thickness of the film were measured using m-line spectroscopy for which a polarised laser beam (632.8 nm) is coupled into the film by means of a rutile prism. For discrete values of the incidence angle, each of the different modes is excited in the film and a dark line is observed in the reflected beam [14].

In the present case, four TE (transverse electric) and four TM (transverse magnetic) modes were observed: from those experiments the effective indexes and the film thickness were deduced [9]. Assuming a step index profile, the mean refractive indexes and the film thickness t were satisfactorily calculated i.e.: $n = 2.228 \pm 0.002$ and $t = 872 \pm 4$ nm for TE modes and $n = 2.249 \pm 0.002$ for TM modes. The thickness value agrees reasonably well with that one estimated from TEM study.

The cut-off index corresponding to the substrate index was determined as 1.735 ± 0.002, which is not significantly different from the value for bulk MgO (1.733). This means that the contribution of the interface region in the present case cannot be detected using m-line spectroscopy, due to its small extent with respect to the film thickness.

4. Discussion

The presence of aluminium seems to be essential to explain the structural and the optical features of the film, as well as those of the film/substrate interface. EDX chemical analysis associated with TEM imaging clearly demonstrates that Al present in the target is kept at the same concentration in the anatase film where no pure Al oxide is detected. Such a rather large concentration of dopant is thought to favour the nucleation of the nanometric size anatase crystallites which form

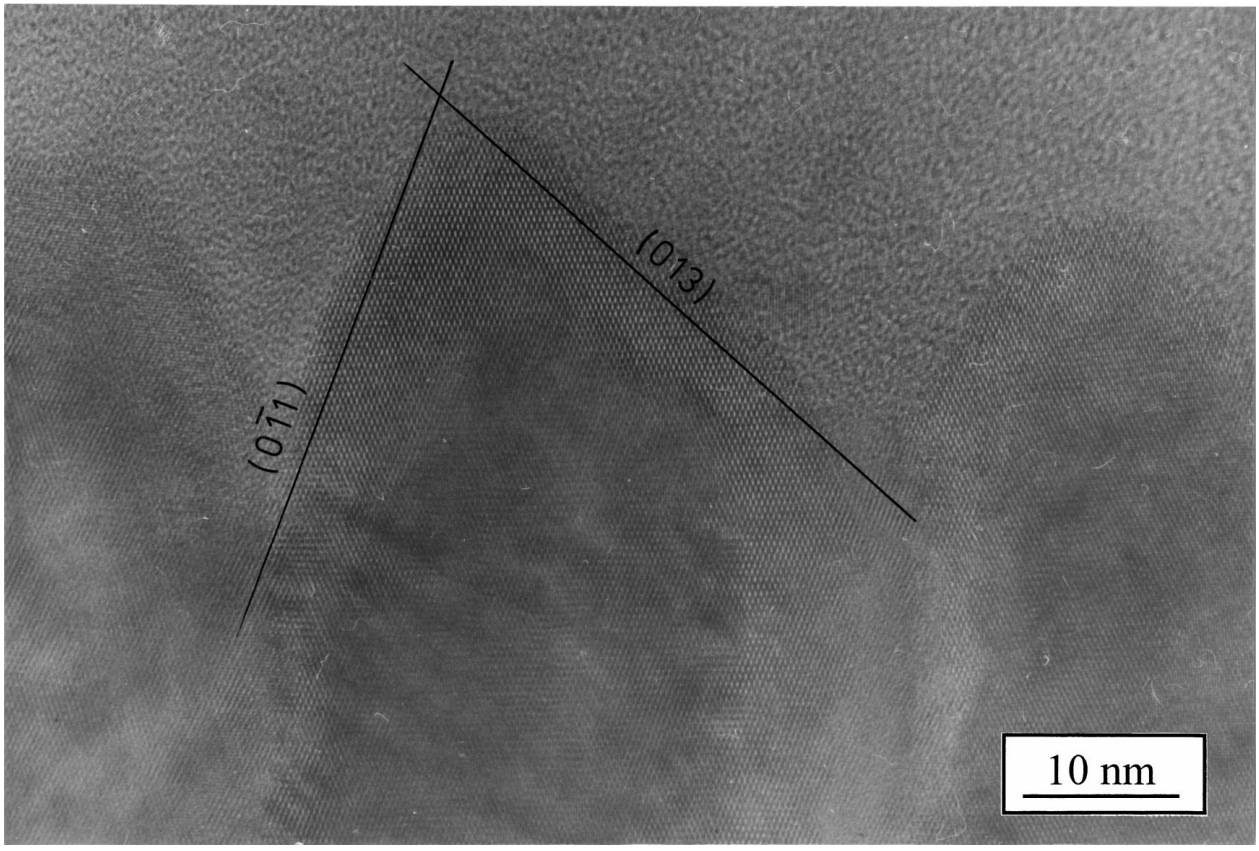

Figure 9 HRTEM image from the top part of the film, showing the surface terminations being parallel to the habit planes of natural anatase.

first on the substrate (and are then imaged as the buffer layer II). The small grain size and the large concentration of dopant are correlated factors that explain stabilisation of anatase structure at the present deposition temperature being nearly the point at which anatase transforms in rutile; this result has been already discussed in a previous paper [8].

The anatase nanocrystallites which form first on the substrate exhibit different orientations with respect to the substrate i.e. the [001] direction of the tetragonal anatase structure can be parallel to any primitive axis of the MgO cubic cell. At a certain thickness (about 20 nm), the actual epitaxial orientation with [001] TiO_2 // [001] MgO, corresponding to the smallest lattice mismatch in the interface plane, becomes predominant and then the columnar growth starts developing. It is thought that the Al dopant can get concentrated in the anatase grain boundaries where an Al rich interphase is thus formed. Due to the large concentration of Al substituted atoms in that phase the normal symmetries of anatase are broken down so that the 001 reflection is activated as mentioned in Section 3.1. The interphase should prevent adjacent grains to coalesce during growth, hence each anatase grain tends to grow independently from the adjacent ones in a columnar process where the column diameter remains nearly constant throughout the film.

The formation of the spinel layer takes place during film deposition by interdiffusion of Mg in TiO_2 and of Ti in MgO. This assumption is based on the uniform contrast observed in the spinel layer, significant of the quite perfectly topotaxial formation of spinel at the film/substrate interface. This mechanism has been evidenced in earlier works [15, 16], where spinel films were obtained directly by sputtering deposition of TiO_2 on MgO crystals heated at temperatures higher than 900 °C. From results obtained at 900 and 1150 °C by Hesse *et al*. [15–17], we can estimate data for interdiffusion of Ti and Mg and spinel formation. Extrapolating these data to the present temperature of 790 °C, it can be stated that the corresponding spinel layer should be at least four times thinner. This leads to the conclusion that the presence of aluminium induces a lower activation energy for interdiffusion and spinel formation. Accordingly the Al atoms will be in excess in the spinel structure, what it is actually observed.

According to the results of EDX analysis (Section 3), two spinel compounds (cubic structure) are thought to occur in the buffer layer: $(Ti,Al)Mg_2O_4$ the substituted form of $TiMg_2O_4$ - magnesium orthotitanate, with $a = 0.844$ nm (JCPDS 3-858), and $(Ti,Al)_2MgO_4$ the substituted form of Ti_2MgO_4 with $a = 0.8474$ nm (JCPDS 16-215). Occurrence of the second phase is theoretically less probable because it implies the existence of Ti^{3+} ions, but it becomes possible due to excess of Al in the spinel region since Al^{3+} does easily substitute Ti^{3+}. The first compound is the most frequent one close to the substrate and the second one close to the anatase film; in the intermediate region of the buffer layer the two spinels coexist separated by antiphase boundaries (APB). Even so the topotactic orientations with respect to the MgO cubic lattice are maintained because of the quasicontinuity of the oxygen sublattice through the interface. The origin of the weak spots

appearing on the SAED patterns like in Fig. 7a, is attributed to the ordering of such APB where Al can get substituted. One possible model, which will be discussed in a separate paper, to explain such an ordered superstructure is based on the same mechanism as that one describing vacancy ordering in nonstoichiometric TiO_{1+x} ($TiO_{1.25}$ for instance) [18]. Indeed diffraction suggests that $TiO_{1.25}$ and its Al substituted forms, $(Ti,Al)_{3.2}O_4$ for instance, are present as minority phases at the bottom part of the columnar region of the film (Section 3.1) and the structure of $(Ti,Al)_{3.2}O_4$ is nearly topotactic with spinel.

The refractive indexes of the film are smaller than those of bulk anatase which are $n_e = 2.561$ for $E \,//\, c$ and $n_o = 2.488$ for $E \perp c$ at a wavelength of 589.3 nm: this is attributed to the contribution of aluminium since the mean index of bulk α-Al_2O_3 is smaller, i.e. $n \approx 1.76$. The index of the film for TE modes (E // film) is significantly smaller than for TM modes ($E \perp$ film); since the lower index of anatase corresponds to $E \perp c$, it can be concluded that the c-axis of anatase in the film is perpendicular to the film surface, in agreement with results of the TEM observations.

5. Conclusions

All the XTEM imaging, diffraction and EDX analysis modes have proved to be useful to determine the structural and chemical features of anatase films deposited by PLD on (001) MgO substrate, as well as those of the film/substrate interface. These investigations reveal that the films have a columnar mosaic texture whose grain size (about 10 nm) indeed requires the spatial resolution of TEM modes for imaging and diffraction. It can be stated that the concentration of the Al dopant present in the target is kept in the film: this explains both the stabilisation of the anatase structure and the columnar texture of the film. The constant diameter columnar growth is attributed to the segregation of Al at the anatase grain boundaries.

The HRTEM imaging mode also has been used to study the film/substrate interface down to nanometer scale. It has been shown that a thin layer (of about 20 nm) of nanocrystallites of anatase is nucleated first at the interface before the favorable epitaxial orientation dominates. On the other side of the interface a buffer layer (of about 30 nm) of spinel is formed by solid state reaction between MgO and TiO_2. Again the presence of Al seems to be essential to explain the formation of the Al rich spinel structure at the temperature of 790 °C: it is suggested that the presence of Al in the lattice lowers the activation energy for the interdiffusion of the metal species in the film/substrate interface region. EDX chemical analysis of the Mg concentration in the spinel layer shows that both the $Mg(Ti,Al)_2O_4$ and $Mg_2(Ti,Al)O_4$ spinels coexist, separated by APB which get ordered locally: a detailed study of that phenomenon will be the matter of a coming paper. Values of the film thickness determined by optical m-lines spectroscopy are consistent with results of the TEM studies; these optical measurements also confirm the influence of the Al dopant. since the refractive indexes are lower than those of non doped anatase.

Acknowledgements

Prof. J. MUGNIER, from LPCML, is gratefully acknowledged for discussions.

References

1. K. BANGE, C. R. OTTERMANN, O. ANDERSON, U. JESCHKOVSKI, M. LAUBE and R. FEILE, *Thin Solid Films* **197** (1991) 279.
2. C. PIRLOG, M. GARTNER, P. OSICIANU, V. S. TEODORESCU, F. MOISE and A. IANCULESCU, *Ceramics International* **22** (1996) 95.
3. J. MUGNIER, B. VARREL, M. BATHAT, C. BOVIER, J. SERUGHETTI, *J. Mater. Sci. Lett.* **11** (1192) 875.
4. W. G. LEE, S. I. WOO, J. C. KIM, S. H. CHOI and K. H. OH, *Thin Solid Films* **237** (1994) 105.
5. S. KING and C. B. CARTER, in Proceedings of the 2nd COLA (Laser Ablation Mechanisms and Application II) AIP Conf. Proc., 1994, p. 288.
6. H. A. DURAND, J. H. BRIMAUD, O. HELLMAN, H. SHIBATA, S. SAKURAGI, Y. MAKITA, D. GESBERT and P. MEYRUEIS, *Appl. Surf. Sci.* **86** (1995) 122.
7. N. LOBSTEIN, E. MILLON, A. HACHIMI, J. F. MULLER, A. ALNOT, J. J. EHRHARDT, *ibid.* **89** (1995) 307.
8. C. GARAPON, C. CHAMPEAUX, J. MUGNIER, G. PANCZER, P. MARCHET, A. CATHERINOT and B. JACQUIER, *ibid.* **96–98** (1996) 836.
9. C. GARAPON *et al.*, submitted.
10. C. CHAMPEAUX, P. MARCHET, J. AUBRETON, J. P. MERCURIO and A. CATHERINOT, *Appl. Surf. Sci.* **69** (1993) 335.
11. V. S. TEODORESCU, M. G. BLANCHIN, C. CHAMPEAUX and C. GARAPON, in "Electron Microscopy 1998," Vol. II, edited by H. A. Calderon Benavides and M. Jose Yacaman (Proc. ICEM 14, Cancun, Mexico, 1998) p. 657.
12. "Electron Microscopy 1998," Vol. I, p. 611, Vol. II, p. 303, Vol. III, p. 561, edited by H. A. Calderon Benavides and M. Jose Yacaman (Proc. ICEM 14, Cancun, Mexico, 1998).
13. M. G. BLANCHIN, V. S. TEODORESCU, J. GARCIA LOPEZ, J. SIEJKA, L. M. MERCANDALLI and R. BISARO, *Phil. Mag. A* **74** (1996) 151.
14. D. ULRICH and R. TORGE, *Appl. Opt.* **12** (1973) 2901.
15. D. HESSE and H. BETHGE, *Journal of Crystal Growth* **52** (1981) 875.
16. *Idem., ibid.* **65** (1983) 69.
17. D. HESSE, *J. Vac. Sci. Technol.* **A 5** (1987) 1696.
18. D. WATANABE, O. TERASAKI and J. R. CASTLES, in "The Chemistry of Extended Defects in Non-Metallic Solids," edited by LeRoy Eyring and Michael O'Keeffe (North-Holland Publishing Company, Amsterdam, London, 1970) pp. 238–258.

Received 28 December 1998
and accepted 9 April 1999